Adaptation to host cell environment during experimental evolution of Zika virus.

Vincent Grass[1], Emilie Hardy[1$], Kassian Kobert[2$], Soheil Rastgou Talemi[3$], Elodie Décembre[1], Coralie Guy[1], Peter V. Markov[2], Alain Kohl[4], Mathilde Paris[5], Anja Böckmann[6], Sara Muñoz-González[1], Lee Sherry[1], Thomas Höfer[3], Bastien Boussau[2]* and Marlène Dreux[1]*

[1] CIRI, Inserm, U1111, Université Claude Bernard Lyon 1, CNRS, UMR5308, École Normale Supérieure de Lyon, Univ Lyon, Lyon, 69007, France

[2] Laboratoire de Biométrie et Biologie Évolutive (LBBE), UMR CNRS 5558, Université Claude Bernard Lyon 1, Lyon, 69622, France

[3] Theoretical Systems Biology, German Cancer Research Center, Deutsches Krebsforschungszentrum (DKFZ) Heidelberg, 69120, Germany

[4] MRC-University of Glasgow Centre for Virus Research, Glasgow G61 1QH, Scotland UK

[5] Institut de Génomique Fonctionnelle de Lyon (IGFL), École Normale Supérieure de Lyon, Lyon, 69007, France

[6] Institut de Biologie et Chimie des Protéines, MMSB, Labex Ecofect, UMR 5086 CNRS, Université de Lyon, Lyon, 69007, France

[$] These authors contributed equally.

* corresponding authors: Marlène Dreux, CIRI, École Normale Supérieure de Lyon, 46 allée d'Italie, 69007, Lyon France, phone : +334 26 23 38 34 and Bastien Boussau, UMR CNRS 5558 - LBBE, UCB Lyon 1 - 43 bd du 11 novembre 1918, 69622 VILLEURBANNE cedex, France, phone : +336 27 64 29 11.

Email: marlene.dreux@ens-lyon.fr Bastien.Boussau@univ-lyon1.fr

Author Contributions: V.G., T.H., B.B. and M.D. designed research; V.G., E.H., K.K., S.R.T., E.D., C.G., P.V.M., M.P., S.M.-G. and L.S. performed research; V.G., E.H., K.K., S.R.T., E.D., C.G., P.V.M., A.K., A.B., M.P., S.M.-G. and L.S. contributed new reagents/analytic tools; V.G., E.H., K.K., S.R.T., E.D., C.G., P.V.M., A.K., M.P., A.B., S.M.-G., L.S., T.H., B.B. and M.D. analyzed data; and V.G., B.B., and M.D. wrote the paper.

Competing Interest Statement: The funders had no role in study design, data collection and analysis, decision to publish, or preparation of the manuscript.

Classification: BIOLOGICAL SCIENCES**;** Microbiology

Keywords: Zika virus; experimental evolution; viral adaptation; mathematical modelling; deep-sequencing analysis.

Abstract

Zika virus (ZIKV) infection can cause developmental and neurological defects and represents a threat for human health. Type I/III interferon responses control ZIKV infection and pathological processes, yet the virus has evolved various mechanisms to defeat these host responses. Here, we established a pipeline to delineate at high-resolution the genetic evolution of ZIKV in a controlled host cell environment. We uncovered that serially passaged ZIKV acquired increased infectivity, defined as the probability for one virus to initiate infection, and simultaneously developed a resistance to TLR3-induced restriction. We built a mathematical model that suggests that the increased infectivity is due to a reduced time-lag between infection and viral replication. We found that this adaptation is cell-type specific, suggesting that different cell environments may drive viral evolution along different routes. Deep-sequencing of ZIKV quasi-species pinpointed mutations whose increased frequencies temporally coincide with the acquisition of the adapted phenotype. We functionally validated a point-mutation in ZIKV envelope (E) protein recapitulating the adapted phenotype. Its positioning on the E structure suggests a putative function in protein refolding/stability. Altogether, our results uncovered ZIKV adaptations to the cell environment leading to an accelerated replication onset coupled with resistance to TLR3-induced antiviral response. Our work provides insights into viral escape mechanisms and interactions with host cell and can serve as a framework to study other viruses.

Significance Statement

Zika virus poses a major threat to Human health worldwide. To understand how Zika virus interacts with human cells, we studied its evolution in cell cultures. We found that the viruses adapted by initiating their replication sooner after cell entry. We sequenced the genomes of the viruses evolved over time and found mutations underlying the adaptation of the virus. One mutation in the envelope viral protein is sufficient to reproduce the faster initiation of replication. Our multidisciplinary approach based on analyzing viral evolution in a controlled environment and mathematical modeling revealed how Zika virus can escape antiviral responses, and can serve as framework to study other viruses.

Introduction

Zika Virus (ZIKV; *Flaviviridae*) is a mosquito-borne human pathogen related to other globally relevant flaviviruses, including dengue, yellow fever, West Nile, Japanese encephalitis and tick-borne encephalitis viruses. As is typical for flaviviruses, ZIKV has a 10.8 kb RNA genome of positive polarity, encoding a polyprotein composed of 3 structural proteins (C, prM and E) and 7 nonstructural (NS) proteins. The NS proteins are involved in the steps of RNA synthesis and assembly of viral particles. Several NS proteins of the flaviviruses interfere with host antiviral responses (1-4).

For decades, ZIKV infections were either unrecognized or occurred only sporadically and were associated with mild symptoms. However, ZIKV was detected in Brazil in 2015 and spread rapidly, reaching infection rates exceeding 50% (5). During the Brazilian ZIKV outbreak, congenital infections lead to fetal demise, microcephaly and other developmental abnormalities, *e.g.*, visual and hearing impairment, skeletal deformities, and Guillain–Barré syndrome in adults (5-9). Severe symptoms, including neural development defects and fetal demise, are linked to host antiviral responses by type I and III interferons (IFN-I/III), which are also central for ZIKV control and *in utero* transmission (10-15). All cells possess signaling pathways designed to trigger the production of IFN-I/III and IFN-stimulated genes (ISGs) upon viral infection. Their effects are potent and wide-ranging: direct inhibition of the viral life cycle at multiple steps and jumpstart of the adaptive immune response. These antiviral responses are induced by the recognition of specific viral motifs by host sensors (*e.g.*, Toll-like receptors) that mobilize cascade signaling. As for other flaviviruses, TLR3-induced signaling reduces ZIKV replication (16). Nonetheless, like virtually all human pathogenic viruses, ZIKA has evolved towards the ability to modulate and counteract the IFN-I/III signaling and other host responses (1-4) likely due to adapted interactions with host

proteins. The mutation rate of ZIKV is expected to be very high, *i.e.*, around $10^{-4/-5}$ mutation per site per replication in accordance with other flaviviruses, since the catalytic site of the NS5 polymerase is well-conserved among flaviviruses (17). This mutation rate ensures a high genetic diversity and adaptability of viral populations. Adaptive mutations that improve the fitness of the virus can do so by improving the viral machinery, optimizing the interactions with proviral host factors, or inhibiting antiviral factors. Given the limited size of the viral genome, trade-offs between these three strategies, and how they play out in the human and mosquito hosts, are expected.

Previous studies on ZIKV evolution mainly focused on the ability of the virus to maintain robust replication in the context of alternate human/mosquito hosts (*e.g.*, (18)). Nonetheless, studies have demonstrated the ability of arboviruses, including ZIKV, to replicate and last for several months in a fraction of infected patients (*e.g.*, detection of viral genome in plasma, urine and semen) (19-24), further stressing out the need to better understand the possible outcome of viral evolution in the human host.

The molecular tracking of arboviral evolution in the host is greatly handicapped by the huge viral diversity due to the error-prone viral polymerase. To overcome this challenge, novel methods for accurate identification of ultra-rare and low-frequency genetic variants in RNA viruses have recently been developed. Especially, the CirSeq method has proved successful to analyze the viral genetic diversity of poliovirus, a viral model known for its high rate of replication (25), as well as the landscape of transcription errors in eukaryotic cells (26).

Here, we adapted this novel methodology to the arbovirus ZIKV, to reveal how it can adapt to the human host cell environment and to reveal the genetic interactions involved. We

conducted an in-depth analysis of the evolution of the viral quasi-species (*i.e.*, population of genomes isolated from infected cell supernatants) through serial passages of an epidemic ZIKV strain in human cell cultures. We uncovered a phenotypic change linked to higher viral spread, *via* increased specific infectivity, which was concomitantly acquired with viral resistance to TLR3-induced antiviral responses. Bioinformatic analyses showed that specific ZIKV variants increased in frequency in temporal association with this phenotypic adaptation, and the corresponding mutations were functionally validated.

Results

Acquisition of increased specific infectivity during experimental evolution.

To uncover the genetic interactions of ZIKV with the host cell environment, we performed experimental evolution in a human cell line. Huh7.5.1 cells were selected as they are a well-characterized cell line deficient for different antiviral sensors, thus offering a stable and well-controlled cell environment (27, 28). Experimental evolution was performed by serial passaging of ZIKV: at each passage, viral populations harvested at 3 days post-infection were used to infect naïve cells (**Fig. 1A**, schema on the left side). Quantification of infectious virus produced over the course of the experimental evolution showed that the viral production increased during serial viral passaging and reached a plateau by days 21-to-27 (**Fig. S1A**). The increased viral productions were observed for all 3 independent runs of experimental evolution and within a similar timeframe (**Fig. S1A**). Likewise, quantifications of intracellular and extracellular viral RNA levels confirmed the augmentation of ZIKV replication over time (**Fig. S1B**).

To address how passaged viral populations adapt to human host cell, we first studied their ability to initiate infection as compared to the parental virus by quantifying the specific infectivity, defined as the probability for one physical virion to initiate infection (determination described in Materials and Methods). We demonstrated an increase of the specific infectivity of the viral populations harvested in the course of all the independent runs of experimental evolution (**Fig. 1A**). The maximum level of specific infectivity was observed by days 21-to-24 in the independent runs of experimental evolutions followed by a plateau, as a likely consequence of viral adaptation to human cells reaching equilibrium. The trend of increased viral production (**Fig. S1A**) appears to be simultaneous and proportioned with the augmentation of specific infectivity (**Fig. 1A**), suggesting that the ability of ZIKV to adapt in this defined host environment primarily occurred *via* an increased capacity to initiate infection.

Increased specific infectivity of passaged virus temporally associates with the resistance to TLR3-induced antiviral response.

Next, we tested the capacity of these passaged viral populations to propagate when submitted to the host antiviral response. Huh7.5.1 cells are known to be deficient for TLR3-induced signaling (28), enabling a specific induction of the antiviral response by complementation *via* ectopic expression of WT TLR3 (**Fig. S1C**). We showed that the treatment of the WT TLR3 expressing cells by poly(I:C), a mimetic of the intermediate double-stranded RNA produced during viral replication, leads to a robust ISG up-regulation at mRNA and protein levels, using ISG15 and MxA as representative ISGs (**Fig. S1D-E**). In contrast, the parental cells (*i.e.*, without ectopic WT TLR3) did not respond to poly(I:C) (**Fig. S1D-E**). This demonstrated that WT TLR3 expression renders our cell model responsive to the TLR3 agonist poly(I:C). Specific control of TLR3-induced ISG response was assessed by the

absence of ISG up-regulation upon poly(I:C) treatment of cells expressing TLR3 with a deletion of the Toll/interleukin-1 receptor (TIR) domain of the cytosolic tail (ΔTIR-TLR3), necessary for recruiting the downstream adaptor (*i.e.*, TIR domain-containing adaptor inducing IFNβ; TRIF) (29) (**Fig. S1C-D**).

Next using this set up, we showed that poly(I:C)-induced TLR3 signaling greatly decreases replication of the parental virus, but not of the passaged viral populations *i.e.*, harvested at day 51 (**Fig. 1B**). Especially, the RNA levels measured at 72 hours post-infection were similar in the TLR3-activated cells *versus* the non-activated cells for the passaged virus (**Fig. 1B**, right curves). We further determined when, in the course of the experimental evolution, ZIKV acquired resistance to TLR3-induced antiviral response. We quantified the inhibition of viral replication by activated-TLR3 signaling for viral populations harvested at different time points (**Fig. S1F**). In keeping with the results shown in **Fig. 1B**, TLR3-induced antiviral response inhibited the parental virus replication by up to 90% at 72 hours post-infection. The resistance to TLR3-mediated inhibition was already observed for the viral populations harvested at 12 days and at the different MOIs applied (**Fig. S1F**).

The resistance to TLR3-induced antiviral response can result from a faster onset of infection by the passaged viral populations. The resulting ongoing replication before the establishment of a robust antiviral response in host cells would out-compete it. In agreement with this hypothesis, when using similar MOI - in the absence of TLR3-induced response - the replication rate of passaged viral populations was significantly faster compared to the parental virus (**Fig. 1B**, comparing the slope from 24-to-48 hours post-infection). Second, the slopes, reflecting the speed of viral expansion for the parental virus were similar with *versus* without antiviral response (**Fig. 1B,** black plain *versus* dotted lines), whereas the passaged viruses expanded more rapidly in the presence of the antiviral inhibition than in its absence (**Fig. 1B,**

blue plain *versus* dotted lines). Similar observations were made for viral populations harvested at distinct late time points of the experimental evolution, including at days 27, 33 and 36 (**Fig. S1G** and *data not shown*). These observations suggest that the passaged viral populations might outcompete host antiviral response by an accelerated infection rate.

Altogether, these results demonstrated that the passaged viral populations acquired an increased capacity for viral spread along with resistance to TLR3-induced antiviral response.

Increased viral replication depends on the targeted cell type but is independent of the ISG response

A faster replication and thus expression of viral proteins compared to host antiviral effectors can result from more efficient interactions and usages of the host machinery by the passaged virus, which may be cell-specific. To test these hypotheses, we assessed the infection efficiency by the passaged virus in different cell environments. First, to assess the infection speed by the passaged viral population compared to the parental virus, we quantified the size of infectious foci formed in a limited timeframe, as reflecting the propagation speed *via* rounds of infection. Foci formed upon infection of Huh7.5.1 cells by the long-term passaged viral population were significantly larger than those formed by parental virus (**Fig. 1C,** left panels and **Fig. S2A**, upper panels). This confirmed the increased infection speed of the viral populations in the cell type used for the experimental evolution. The opposite was observed in a distinct cell line, *i.e.*, the simian Vero cells (**Fig. 1C and S2A,** left panels). To further analyze this cell type-specific phenotype, we performed a kinetic analysis of viral replication. The replication rate of passaged viral populations significantly increased *i.e.*, approx. 10 fold-increase as compared to parental virus in Huh7.5.1 cells (**Fig. 1D**, upper panel), with similar ZIKV RNA levels observed early after infection, likely reflecting the viral input. In contrast, the replication rates of the adapted viral population did not increase compared to the parental

virus in Vero cells (**Fig. 1E,** upper panel). The kinetic analysis of the ISG response (representative MxA and ISG56 mRNAs) demonstrated a difference between the cell types (**Fig. 1D-E,** lower panels and **Fig S2C-D**). An early ISG response was triggered upon infection of Huh7.5.1 cells by parental virus, yet only observed with high MOI, and vanished for the viral populations harvested later in the course of the experimental evolution (**Fig. 1D and S1G-H**). In Vero cells, infection by either viral populations led to similar ISG responses (**Fig. 1E** and **S2D**). This differential profile of ISG response between the two cell types might result from the absence in Vero cells of a response to an activating signal contained in the supernatants harvested at early time-points of the experimental evolution, or alternatively from a qualitatively and/or quantitatively different cell entry pathway in these cell types.

To discriminate these possibilities, we broadened this phenotypic analysis to alternative human cell types. Similar to Huh7.5.1 cells, the replication rate of adapted viral populations was significantly increased in HEK-293 cells compared to the parental virus (**Fig. 1F**, upper panel). Unlike Huh7.5.1 cells, neither parental virus nor adapted viral populations induced an ISG response in HEK-293 cells (**Fig. 1F** and **S2E**), indicating that higher replication rate of the adapted viral populations *versus* parental virus can occur independently of an ISG response. The results also demonstrated that the increased propagation rate of the adapted viral populations is not restricted to a unique cell type.

To further confirm that the increased infection rate by the adapted viral population was independent from the early ISG response, we compared the viral replication kinetics in both U6A cells deficient for STAT2 (*i.e.,* an ISG transcription regulator of the signaling pathway induced by IFN-I and III), and U6A cells complemented for STAT2 expression, referred to as STAT2-U6A cells (**Fig. 1G,** upper panels). STAT2 expression potentiates the ISG response upon ZIKV infection with an accelerated response observed at 48 hours post-infection in STAT2-U6A cells as opposed to the poor response of the corresponding U6A cells (**Fig. 1G ,**

and **S2F**) and consistently, a decreased viral replication in STAT2-U6A cells compared to the corresponding U6A cells (**Fig. 1G**, comparing the upper panels). We showed that, in either the U6A cells or STAT2-U6A cells, the levels of both viral replication and the ISG response were similar for the adapted *versus* the parental viral populations (**Fig. 1G**). Taken together our results obtained in cell types failing to respond to ZIKV infection by ISG up-regulation (*i.e.*, HEK-293) or competent for ISG induction (STAT2-U6A cells) suggested that the increased infection rate of the adapted viral populations is independent of the extent of ISG up-regulation.

We also tested the rate of viral replication in macrophages differentiated from monocytes isolated from healthy human blood donors (**Fig. 1H** and **S2B**), representing a cell model closely related to the cell type targeted *in vivo* by ZIKV (30-33). Interestingly, we observed that the propagation of the passaged viral populations was significantly abrogated in this cellular model as compared to the parental virus (**Fig. 1H**). ISG induction was readily detected in response to the parental virus, but not for the passaged viral population (**Fig. 1H and S2G**).

Altogether, these comparative analyses using different cell types suggested that the viral adaptations lead to higher infection rate independently of the ISG response, thus suggesting that the ability of passaged viral populations to initiate infection most likely involves viral-host interactions and entry pathways that depend on the cellular environment.

Genetic diversity and evolution of the viral populations determined by deep-sequencing analysis.

To delve into the mechanism underlying the viral adaptation, we analyzed the genomic diversity of the viral populations harvested in the course of these evolutionary experiments. Conventional sequencing methods provide consensus sequences and cannot detect low

frequency variants, which can nevertheless be very important functionally. To bypass this limitation and generate data of sufficient depth to characterize virus populations, we set up a kinetic analysis by deep-sequencing the entire genomes of the viral populations sampled at various time points of the experimental evolution. Our methodology was adapted from the "CirSeq" method that reduces next-generation sequencing errors (25). The bioinformatic analyses revealed that CirSeq was successful, with tandem repeat occurrence ranging from 59% to 94% (mean 84%) per read, and repeat sizes ranging from 33 to 97 bases (mean size 50 to 60 bases). The sequences are available in SRA with accession numbers SRX9704326-SRX9704344; bioproject PRJNA686429. In addition, the coverage quantification revealed that our methodology using 200-PE runs with HiSeq 2500XL led to a read number/depth as high as 2x10E5 (**Fig. 2A** and **S3A**). Minimal coverage (*i.e.*, read numbers below 1000) was found at only 55 positions out of all the analyzed libraries and the mean coverage per position across all analyzed experimental conditions ranged from approx. 10E4 to 10E5 (**Fig. S3B**), thus allowing an in-depth analysis of the different viral populations. Moreover, the profiles of viral genome coverage across all analyzed samples were similar (**Fig. 2A and S3A**). These results thus validated the reproducibility of our experiments and implied that composition and/or secondary structure of certain viral genome segments had a limited impact on the sequencing analysis.

Next, we studied the viral diversity over-time, *i.e.*, mutation frequencies over the course of the independent runs of experimental evolution (**Fig. 2B-C** and **S3C**). We validated that the major variant obtained by deep-sequencing of the inoculum used for our experimental evolutions perfectly matches the clinical isolate (GenBank ID KX197192). To identify mutations whose frequency significantly varied through time, for each experiment, we computed position-wise standard deviations of the frequency of the most frequent variant. As

shown in **Fig. S4A**, the standard deviations are distributed in two categories: *i/* a high density of very low frequency variants, likely corresponding to polymorphisms due to the error-prone feature of the NS5 polymerase and/or generated during library preparation, despite the CirSeq protocol and *ii/* low density of polymorphisms showing higher standard deviations, corresponding to mutations that have reached a high frequency during at least one time-point of one experiment. Further investigation of the variants with standard deviation above a threshold of 0.1 or 0.02 showed that 4 or 7 variants, respectively, had high standard deviations in several independent experiments (**Fig. S4B-C).** Focusing on the highest threshold and/or on substitutions appearing in different independent experiments, 6 variants are spread across the genome, and reach high frequencies over the course of several experiments (**Fig. 2** and **S3C,** marked by grey lines, and **S4B**). We provide a representation of variant frequencies at day 18 that highlights the similarity of the frequency profiles between independent experiments (**Fig. 2C**).

Identification of candidate adaptive mutations in ZIKV E and NS4B proteins.

We further analyzed the mutations that passed the standard deviation thresholds, considering them as candidate adaptive mutations (**Fig. 2D-F and S4B-C**). Among the 4 variants that passed the 0.1 threshold, 3 positions do so in a number (n) = 3 of experiments (*i.e.*, 1786, 2341, 7173); 1 additional position does so in n = 2 (*i.e.*, 2194) (**Fig. 2D-E**). Additional positions are found when the threshold is set to 0.02 for n = 3 (*i.e.*, 5663, 10007) (**Fig. 2F**). Among these variants, some are synonymous mutations within the coding part of the ZIKV polyprotein, and others appear in a limited number of samples and/or are not concomitant to the phenotypic adaptation (*i.e.*, position 2194, **Fig. 2E**). The non-synonymous C1786T mutation, leading to the reversion at position 270 of E envelope protein from V to A and

present in the clinical isolate (ZIKV PE243, KX197192) (34), had a high frequency at the beginning of the experiments, likely resulting from the initial viral amplification in Vero cells.

The frequency of the C2341T mutation increased from days 6-to-12 (**Fig. 2D**), thus preceding both the augmented specific infectivity and the acquisition of resistance to TLR3-induced antiviral response and (**Fig. 1A and S1A-B**). This corresponds to a mutation of amino acid S-to-L, at position 455 of the E envelope protein. Likewise, the frequency of T7173C was observed as early as day 9 in some experiments and becomes the majority variant by day 18-to-24 in the independent experiments (**Fig. 2D**). This corresponds to a Y-to-H mutation at position 87 in the NS4B protein. These mutations were observed in viral populations harvested from all the independent experiments (**Fig. 2D**). Together, the bioinformatic analyses of the viral genomes at different time points during experimental evolution underscored the repeated increases in frequency of point mutations in E and NS4B proteins, temporally correlating the phenotype of viral adaptation defined in the course of the independent runs of experimental evolution.

The S455L mutation in the E viral protein recapitulates both the increased specific infectivity and the resistance to TLR3 antiviral response.

To functionally validate the candidate adaptive mutations, the S455L mutation in the E envelope protein and the Y87H mutation in NS4B were introduced alone or combined in a corresponding recombinant ZIKV. First, we generated a ZIKV molecular clone (referred to as 'ref no mut') corresponding to the clinical isolate used for experimental evolution by introducing R99G and Y122H mutations in NS1 in the previously reported molecular clone BeH819015 (35). Of note, we showed the absence of significant impact of these NS1 mutations on viral spread and specific infectivity (**Fig. S5A-C**).

The efficiency of transfection of the different mutants was comparable to that of the reference, as determined by ZIKV intracellular levels at 6 hours post-transfection (**Fig. S5G**). While the Y87H mutation in NS4B showed no significant difference as compared to the reference (ref no mut), the S455L mutation in the E protein significantly increased the rate of viral replication when present alone or in combination with Y87H in NS4B (**Fig. 3A**). The S455L mutation in E also recapitulated the enhanced specific infectivity observed for viral populations evolved in the course of the evolution experiments (compare **Fig. 3B** to **1A**).

We further showed that the size of infectious foci formed in a limited timeframe (*i.e.*, reflecting the speed of viral propagation *via* new rounds of infection, as in **Fig. 1C**) significantly increased upon infection with the E S455L mutant as compared to the reference in Huh7.5.1 cells (**Fig. 3C** and **S5H,** left panels). In contrast, the size of infectious foci formed upon infection by E S455L mutant was reduced as compared to the reference in Vero cells (**Fig. 3C** and **S5H,** right panels). This is consistent with the observations for the viral populations adapted in the course of experimental evolution (**Fig. 1C**). We demonstrated that, similar to the adapted viral populations obtained in the experimental evolutions, the E S455L mutant resists inhibition by TLR3-induced antiviral response (**Fig. 3D**, right curves), as opposed to the reference molecular clone (**Fig. 3D**, left curves). Altogether, our results demonstrated that the S455L point mutation located in proximity to the trans-membrane domain of ZIKV E protein and interacting with membrane lipid and/or with the viral protein M (**Fig. S7**) recapitulates the phenotype observed with the adapted viral population.

Given that the E S455L mutation causes improved viral replication both in the presence and absence of TLR3-induced signaling, we asked whether an accelerated onset of replication

could provide a unifying mechanism. To this end, we modeled this mechanism mathematically and compared the model results with our experimental data. The model (**Fig. 4A**) describes the infection of susceptible cells, which, after a time delay, enter a phase of productive replication. Produced infectious virions can then infect other susceptible cells. Individual cells in this multiscale model will have their own time course of ZIKV replication, depending on the time of infection (**Appendix 1, mathematical model**). We determined the kinetic parameters of the model (including infection rate, delay to productive replication, replication rate, virion production rate and infection-induced cell death rate) by fitting the model to two sets of experimental data (**Fig. 3 and S1G)**. The effects of both evolution and introduction of the E S455L point mutation were modeled by allowing the delay to productive replication to be different from parental and reference strains, respectively, keeping all other parameters identical. The model captured the data (**Fig. 4B-C**) with a well-constrained set of parameter values **(Fig. S6)**. The delay to productive replication was shortened from around 8 hours for the (parental or reference) controls to 6 hours or less for the adapted or mutated strains (**Fig. 4D**). Our model thus suggests that the E S455L mutation allows a reduced time-lag between infection and viral replication, which suffices to cause increased virus spread, and probably the associated resistance to the TLR3-induced antiviral response.

Discussion

Experimental evolution in a stable and controlled cell environment uncovered ZIKV adaptations leading to the avoidance of induced host antiviral response *via* an increased specific infectivity. Bioinformatic analysis of the viral evolution pinpointed candidate viral determinants, whose frequencies increased concomitantly with the acquisition of the adapted phenotype. We further showed that viral adaptation augmented infection independently of the

ISG response and in specific cellular environments, thus suggesting a modulation of the host-virus interaction involved at the early step of ZIKV infection. Consistently, we uncovered a key determinant in the envelope (E) protein that both augments the probability for one physical virus to initiate infection in certain cell environments and allows resistance to the TLR3-induced antiviral response.

Proposed mechanism for the resistance to antiviral response

Since the acquisition of both increased specific infectivity and resistance to TLR3-induced antiviral response were temporally associated during the experimental evolution, and knowing that the E S455L point mutation reproduces both phenotypes, we propose that the two phenotypes are causally linked. Like other flaviviruses, ZIKV has evolved inhibitory mechanisms against antiviral responses, including blockage of the response to type I and III IFNs by NS5-mediated degradation of STAT2 (1-4). Our results suggest that viral adaptation occurs *via* a reduction of the time delay prior to the onset of productive infection rather than by directly modulating virus-mediated inhibition of the host antiviral detection. First, we showed that improved viral replication of the adapted populations was independent of the amplitude of the ISG response, as demonstrated using HEK-293 where the ISG up-regulation is absent. Second, the comparison of the U6A-STAT2 cells *versus* the corresponding U6A cells (*i.e.*, STAT2 deficient) indicated that the adapted viral populations did not differentially inhibit ISG responses induced by Jak/STAT signaling compared to the parental virus. Third, the kinetic analysis demonstrated that the adapted viral populations showed enhanced resistance to TLR3-mediated inhibition at later time-points post-infection, and with higher viral input. Fourth, our mathematical model of ZIKV infection and replication showed that a reduced time-lag prior to the establishment of productive infection suffice to cause increased virus spread, and hence the associated resistance to the antiviral response. In accordance with

the model, we demonstrated an increased specific infectivity of the adapted viral populations and E S455L mutated recombinant virus, suggesting adaptation of host-ZIKV interaction at the early step of infection.

As this viral adaptation is cell type-restricted, the adapted viral populations likely become fitter by interacting with host factors preferentially present or conversely at a limiting level in certain cell types at early stages of infection (*e.g.*, some characteristic of the entry pathway including endosome acidification and/or AXL receptor) (36-38). Overall our results indicated that the observed viral adaptation most likely results from an improved ability to rapidly and efficiently establish viral replication. Hence a faster accumulation of viral products in newly infected cells can overwhelm and/or bypass the host antiviral factors.

Identification of a key determinant in ZIKV E responsible for increased specific infectivity.

The bioinformatic analysis identified the mutations S455L in E and Y87H in NS4B as reproducibly associated to the adapted phenotype. The high mutation rate of ZIKV allowed the same mutation to appear in several replicates; then, the strong fitness benefits this mutation provided in the cell environment allowed it to rise in frequency through selection. The functional analysis by insertion of the candidate mutations in a ZIKV molecular clone demonstrated that the S455L mutation in E is a pivotal viral determinant controlling both improved viral spread and resistance to TLR3-induced antiviral signaling, probably through accelerated replication onset according to our mathematical model.

The cellular study model has a reduced complexity compared to whole organisms (*e.g.*, unique cell type, restricted diversity of antiviral sensing and absence of adaptive response and physico-chemical constraints such as blood flow). This enabled the discovery of viral

435 adaptation improving fitness in a stable and well-defined cell environment without trade-offs
436 caused by alternative virus/host interactions (39, 40). At the organism scale, interferences
437 between several selective pressures could impede the acquisition of some optimized
438 interaction(s). This may explain why the adaptive mutation at position 455 of the E envelope
439 protein is found in a very limited number of isolates in the ZIKV database of sequences
440 isolated from patients (*i.e.*, only in 2 out of 519 ZIKV full genome sequences issued from
441 patients; NCBI Virus Variation Resource on December 21 2020) and is not maintained in a
442 mutational scanning using a different cell type and strain (41). Alternatively, adaptive
443 mutations may enable the virus to infect different cell types with differential efficiency. In
444 this scenario, the most frequent ZIKV variants would be well adapted to infect the major
445 target cell types, while low-frequency variants would be better at infecting specific cell types.
446 In accordance with this, comparison between various cell types showed that the adapted
447 phenotype is cell type-restricted, indicating that the targeted host factor is differentially
448 involved in viral replication depending on the cell type. This also suggests cell type-specific
449 trade-offs for the virus: adaptation to a particular cell environment limits infectivity in other
450 cellular environments.
451
452 The position 455 is located at the C-terminus of the stem region, next to the transmembrane
453 domain of the E protein (42-44). In the structure of E (5ire.pdb reference) (44), the position
454 455 is located near the membrane surface, in an environment of nearly exclusively polar and
455 hydrophobic residues (**Fig. S7**). Its side chain hydroxyl does not show interactions with the
456 transmembrane helix of the M protein facing it, but is likely involved in lipid headgroup
457 interactions. A mutation from polar to hydrophobic in this region thus has the potential to
458 change the membrane anchorage and insertion of the protein. The *in silico* estimation of the
459 structural changes induced by the S455L mutation suggested that this adaptive mutation

might enhance the stability of the E protein *via* its interaction with apposed segments in M or, more likely, with specific membrane lipids (**Fig. S7**). Consistent with the known regulatory function of this segment in flaviviruses (42-47), we propose that the E S455L mutation modulates the membrane fusion process and/or E protein membrane incorporation. Thus, albeit future analysis is required to test this hypothesis, the structural property of the E S455L mutation is in agreement with the demonstration of an ability to better initiate de novo infection (*i.e.,* increased specific infectivity) of the E adaptive mutant. Therefore, we propose a working model of viral adaptation *via* an optimized interaction with the host machinery involved at an early stage of infection, via E membrane interactions, and likely by modulating its function in membrane fusion. In turn, higher infectivity would result in the accelerated accumulation of viral products and/or altered entry pathway that overcome or bypass host antiviral responses.

In conclusion, we established a framework to study viral adaptation in a stable and controlled cellular environment leading to outcomes (*i.e.,* mutation and phenotype) reproducibly observed in independent runs of experimental evolution. The novel methods of deep sequencing and bioinformatics set up here allowed the identification of mutations at low frequency arising across the entire viral genome, as expected for RNA viruses with a high error rate during replication. The profiles of frequency increase of the variants suggested that they were *bona fide* variants, not experimental artifacts of our sequencing protocol. Focusing on the mutations that reached high frequency and whose increased frequency is temporally associated to the adapted phenotype, we functionally validated one of them by recapitulating the observed phenotypes, thus showing the power of our approach combining viral evolution, mathematic modeling and functional assays. Looking forward, our approach can serve as a framework to study viral interactions with host restriction mechanisms and uncanonical cell entry pathways as well as antiviral strategies.

Material and Methods

Biological materials

Huh7.5.1 cells, Vero E6 cells, U6A cells expressing or not human STAT2 (reciprocally kindly provided by Dr F.V. Chisari, Scripps Research Institute; Dr M Bouloy, Institut Pasteur; Dr M. Ko□ster, Helmholtz-Zentrum für Infektionsforschung) and HEK-293 cells (ATCC CRL-1573) were cultured as previously described (48, 49). Monocytes were isolated from blood from healthy adult human volunteers, obtained according to procedures approved by the 'Etablissement Français du sang' (EFS) Committee. Monocytes were positively selected using anti-CD14 microbeads (MACS Miltenyi Biotec) from PBMCs isolated using Ficoll-Hypaque density centrifugation. The details of the reagent, culture, infections, analysis of viral replication and spread along with the statistical analysis of viral parameters are decrsibed in SI Materials and Methods. To get a controlled set up for the evolutionary experiment and in line with our strategy to work in a cell environment non-responsive to viral products, we used Huh7.5.1. In addition, to enable the subsequent study of the influence of activated antiviral response on the evolved ZIKV populations (*i.e.*, TLR3-induced signaling by poly(I:C) treatment), we transduced Huh7.5.1 cells with a WT TLR and as reference control: a mutant TLR3 invalidated for signaling via a deletion of the Toll/interleukin-1 receptor (TIR) domain of the cytosolic tail (ΔTIR-TLR3) (28, 29). The retroviral-based vectors expressing WT TLR3 and ΔTIR-TLR3 were produced in HEK-293T cells and used to transduce Huh7.5.1 cells, as we previously described (50).

Serial passaging of viral populations, deep sequencing and bioinformatic analysis for the selection of variants.

A clinical isolate of ZIKV from Brazil collected from a patient during the epidemics (PE243_KX197192) was amplified using Vero E6 cells (34). The serial passaging of viral populations was performed by inoculation of Huh7.5.1 cells expressing ΔTIR TLR3 as detailed in SI Materials and Methods. At the indicated time, supernatants were harvested from the infected cells, and multiplexed Illumina libraries for deep sequencing generated from extracted RNA via tandem repeats of the fragment to reduce the error rate of next-generation sequencing (25) were sequenced using HiSeq 2500XL (Illumina), using a 200-PE run at the EMBL Genecore Facility (Heidelberg, Germany).

Reads were quality-checked and trimmed of sequencing adapters and then mapped using PEAR (51) and in-house software (https://github.com/Kobert/viroMapper) as detailed in SI Materials and Method. To detect variants of interest, for each site and in each experiment, we computed the standard deviation of the frequency of the major variant, as represented in **Fig. S4A**. A Jupyter notebook reproducing these analyses will be made available upon publication.

Introduction of selected mutation and analysis of adapted mutants in the ZIKV infectious clone.

Mutations were introduced in the genomic length ZIKV infectious clone cDNA, pCCI-SP6-ZIKV BeH819015 plasmid (35). For adequate comparison with clinical isolate PE243 (34), the R99G and Y122H mutations in NS1 were introduced in pCCI-SP6-ZIKV BeH819015 plasmid. The introduction of the mutants, the preparation of *in vitro* RNA transcripts and analysis of viral replication are described in SI Materials and Method.

Acknowledgements

We thank P. Despres (PIMIT, Université de La Réunion-INSERM France) for the anti-E 4G2 antibody; F.V. Chisari (Scripps Research Institute, La Jolla, CA) for Huh-7.5.1 cells; Dr M

Bouloy (Institut Pasteur, Paris, France) for Vero E6 cells and by Dr M. Ko□ster (Helmholtz-Zentrum für Infektionsforschung) for U6A cells. We are grateful to Y. Jaillais for critical reading of the manuscript. We acknowledge the contribution of SFR Biosciences (UMS3444/CNRS, US8/Inserm, ENS de Lyon, UCBL) facilities. This work was supported by grants from the “Agence Nationale pour la Recherche” (ANR-JCJC-EXAMIN), the ‘‘Agence Nationale pour la Recherche contre le SIDA et les Hépatites Virales’’ (ANRS-AO 2017-01), the European Union's Horizon 2020 Research and innovation program under “ZIKALLIANCE” (Grant Agreement no. 734548) to MD. The grants from “Fondation pour la recherche médicale’’ (contract Bioinformatic analysis for research in biology, DBI20141231313 and from the “Agence Nationale pour la Recherche” LabEx Ecofect (Grant ANR-11-LABX-0048) to MD, BB and AB. AK is supported by the UK Medical Research Council (MC_UU_12014/8, MR/N017552/1).

References

1. M. G. Zimmerman *et al.*, STAT5: a Target of Antagonism by Neurotropic Flaviviruses. *Journal of virology* **93** (2019).
2. T. M. Serman, M. U. Gack, Evasion of Innate and Intrinsic Antiviral Pathways by the Zika Virus. *Viruses* **11** (2019).
3. W. Riedl *et al.*, Zika Virus NS3 Mimics a Cellular 14-3-3-Binding Motif to Antagonize RIG-I- and MDA5-Mediated Innate Immunity. *Cell host & microbe* **26**, 493-503 e496 (2019).
4. B. Wang *et al.*, Structural basis for STAT2 suppression by flavivirus NS5. *Nat Struct Mol Biol* **27**, 875-885 (2020).
5. P. Brasil *et al.*, Zika Virus Outbreak in Rio de Janeiro, Brazil: Clinical Characterization, Epidemiological and Virological Aspects. *PLoS Negl Trop Dis* **10**, e0004636 (2016).
6. V. M. Cao-Lormeau *et al.*, Guillain-Barre Syndrome outbreak associated with Zika virus infection in French Polynesia: a case-control study. *Lancet* S0140-6736(16)00562-6 [pii]
10.1016/S0140-6736(16)00562-6 (2016).
7. W. K. de Oliveira *et al.*, Infection-related microcephaly after the 2015 and 2016 Zika virus outbreaks in Brazil: a surveillance-based analysis. *Lancet* **390**, 861-870 (2017).
8. D. F. Robbiani *et al.*, Risk of Zika microcephaly correlates with features of maternal antibodies. *The Journal of experimental medicine* jem.20191061 [pii]
10.1084/jem.20191061 (2019).
9. F. R. Cugola *et al.*, The Brazilian Zika virus strain causes birth defects in experimental models. *Nature* **534**, 267-271 (2016).
10. L. J. Yockey *et al.*, Type I interferons instigate fetal demise after Zika virus infection. *Sci Immunol* **3** (2018).
11. C. Li *et al.*, Zika Virus Disrupts Neural Progenitor Development and Leads to Microcephaly in Mice. *Cell Stem Cell* S1934-5909(16)30084-4 [pii]
10.1016/j.stem.2016.04.017 (2016).
12. E. A. Caine *et al.*, Interferon lambda protects the female reproductive tract against Zika virus infection. *Nat Commun* **10**, 280 (2019).
13. B. W. Jagger *et al.*, Gestational Stage and IFN-lambda Signaling Regulate ZIKV Infection In Utero. *Cell host & microbe* **22**, 366-376 e363 (2017).
14. J. J. Miner *et al.*, Zika Virus Infection during Pregnancy in Mice Causes Placental Damage and Fetal Demise. *Cell* **165**, 1081-1091 (2016).
15. J. Dang *et al.*, Zika Virus Depletes Neural Progenitors in Human Cerebral Organoids through Activation of the Innate Immune Receptor TLR3. *Cell Stem Cell* S1934-5909(16)30057-1 [pii]
10.1016/j.stem.2016.04.014 (2016).
16. R. Hamel *et al.*, Biology of Zika Virus Infection in Human Skin Cells. *Journal of virology* **89**, 8880-8896 (2015).
17. M. Bollati *et al.*, Structure and functionality in flavivirus NS-proteins: perspectives for drug design. *Antiviral Res* **87**, 125-148 (2010).
18. L. A. Moser *et al.*, Growth and adaptation of Zika virus in mammalian and mosquito cells. *PLoS Negl Trop Dis* **12**, e0006880 (2018).
19. L. Barzon *et al.*, Virus and Antibody Dynamics in Travelers With Acute Zika Virus Infection. *Clin Infect Dis* **66**, 1173-1180 (2018).

20. M. Stone *et al.*, Zika virus RNA and IgM persistence in blood compartments and body fluids: a prospective observational study. *Lancet Infect Dis* S1473-3099(19)30708-X [pii]
10.1016/S1473-3099(19)30708-X (2020).
21. A. Sanchez-Montalva, F. Salvador, I. Molina, Persistence of Zika Virus in Body Fluids - Final Report. *N Engl J Med* **380**, 198 (2019).
22. G. Paz-Bailey, E. S. Rosenberg, T. M. Sharp, Persistence of Zika Virus in Body Fluids - Final Report. *N Engl J Med* **380**, 198-199 (2019).
23. J. J. Hoarau *et al.*, Persistent chronic inflammation and infection by Chikungunya arthritogenic alphavirus in spite of a robust host immune response. *J Immunol* **184**, 5914-5927 (2010).
24. S. Ozden *et al.*, Human muscle satellite cells as targets of Chikungunya virus infection. *PLoS ONE* **2**, e527 (2007).
25. A. Acevedo, L. Brodsky, R. Andino, Mutational and fitness landscapes of an RNA virus revealed through population sequencing. *Nature* **505**, 686-690 (2014).
26. J. F. Gout *et al.*, The landscape of transcription errors in eukaryotic cells. *Sci Adv* **3**, e1701484 (2017).
27. R. Sumpter *et al.*, Regulating intracellular antiviral defense and permissiveness to hepatitis C virus RNA replication through a cellular RNA helicase, RIG-I. *Journal of virology* **79**, 2689-2699 (2005).
28. N. Wang *et al.*, Toll-like receptor 3 mediates establishment of an antiviral state against hepatitis C virus in hepatoma cells. *Journal of virology* **83**, 9824-9834 (2009).
29. L. Alexopoulou, A. C. Holt, R. Medzhitov, R. A. Flavell (2001) Recognition of double-stranded RNA and activation of NF-kappaB by Toll-like receptor 3. in *Nature*, pp 732-738.
30. A. F. Carlin *et al.*, Deconvolution of pro- and antiviral genomic responses in Zika virus-infected and bystander macrophages. *Proceedings of the National Academy of Sciences of the United States of America* **115**, E9172-E9181 (2018).
31. K. A. Jurado *et al.*, Zika virus productively infects primary human placenta-specific macrophages. *JCI Insight* **1** (2016).
32. J. Lang *et al.*, An hPSC-Derived Tissue-Resident Macrophage Model Reveals Differential Responses of Macrophages to ZIKV and DENV Infection. *Stem Cell Reports* **11**, 348-362 (2018).
33. K. M. Quicke *et al.*, Zika Virus Infects Human Placental Macrophages. *Cell host & microbe* **20**, 83-90 (2016).
34. C. L. Donald *et al.*, Full Genome Sequence and sfRNA Interferon Antagonist Activity of Zika Virus from Recife, Brazil. *PLoS Negl Trop Dis* **10**, e0005048 (2016).
35. M. Mutso *et al.*, Reverse genetic system, genetically stable reporter viruses and packaged subgenomic replicon based on a Brazilian Zika virus isolate. *The Journal of general virology* **98**, 2712-2724 (2017).
36. J. Chen *et al.*, AXL promotes Zika virus infection in astrocytes by antagonizing type I interferon signalling. *Nat Microbiol* **3**, 302-309 (2018).
37. E. G. Acosta, V. Castilla, E. B. Damonte, Alternative infectious entry pathways for dengue virus serotypes into mammalian cells. *Cell Microbiol* **11**, 1533-1549 (2009).
38. M. F. Wells *et al.*, Genetic Ablation of AXL Does Not Protect Human Neural Progenitor Cells and Cerebral Organoids from Zika Virus Infection. *Cell Stem Cell* **19**, 703-708 (2016).
39. Y. Arai *et al.*, Novel Polymerase Gene Mutations for Human Adaptation in Clinical Isolates of Avian H5N1 Influenza Viruses. *PLoS Pathog* **12**, e1005583 (2016).

643 40. B. S. Chambers, Y. Li, R. L. Hodinka, S. E. Hensley, Recent H3N2 influenza virus
644 clinical isolates rapidly acquire hemagglutinin or neuraminidase mutations when
645 propagated for antigenic analyses. *Journal of virology* **88**, 10986-10989 (2014).
646 41. M. Sourisseau *et al.*, Deep Mutational Scanning Comprehensively Maps How Zika
647 Envelope Protein Mutations Affect Viral Growth and Antibody Escape. *Journal of*
648 *virology* **93** (2019).
649 42. V. A. Kostyuchenko *et al.*, Structure of the thermally stable Zika virus. *Nature* **533**,
650 425-428 (2016).
651 43. V. M. Prasad *et al.*, Structure of the immature Zika virus at 9 A resolution. *Nat Struct*
652 *Mol Biol* **24**, 184-186 (2017).
653 44. D. Sirohi *et al.*, The 3.8 A resolution cryo-EM structure of Zika virus. *Science (New*
654 *York, N.Y* **352**, 467-470 (2016).
655 45. D. E. Klein, J. L. Choi, S. C. Harrison, Structure of a dengue virus envelope protein
656 late-stage fusion intermediate. *Journal of virology* **87**, 2287-2293 (2013).
657 46. X. Zhang *et al.*, Cryo-EM structure of the mature dengue virus at 3.5-A resolution.
658 *Nat Struct Mol Biol* **20**, 105-110 (2013).
659 47. K. Stiasny, S. Kiermayr, A. Bernhart, F. X. Heinz, The membrane-proximal "stem"
660 region increases the stability of the flavivirus E protein postfusion trimer and
661 modulates its structure. *Journal of virology* **87**, 9933-9938 (2013).
662 48. E. Decembre *et al.*, Sensing of immature particles produced by dengue virus infected
663 cells induces an antiviral response by plasmacytoid dendritic cells. *PLoS Pathog* **10**,
664 e1004434 (2014).
665 49. T. Frahm, H. Hauser, M. Koster, IFN-type-I-mediated signaling is regulated by
666 modulation of STAT2 nuclear export. *Journal of cell science* **119**, 1092-1104 (2006).
667 50. M. Dreux *et al.*, Short-range exosomal transfer of viral RNA from infected cells to
668 plasmacytoid dendritic cells triggers innate immunity. *Cell host & microbe* **12**, 558-
669 570 (2012).
670 51. J. Zhang, K. Kobert, T. Flouri, A. Stamatakis, PEAR: a fast and accurate Illumina
671 Paired-End reAd mergeR. *Bioinformatics* **30**, 614-620 (2014).
672

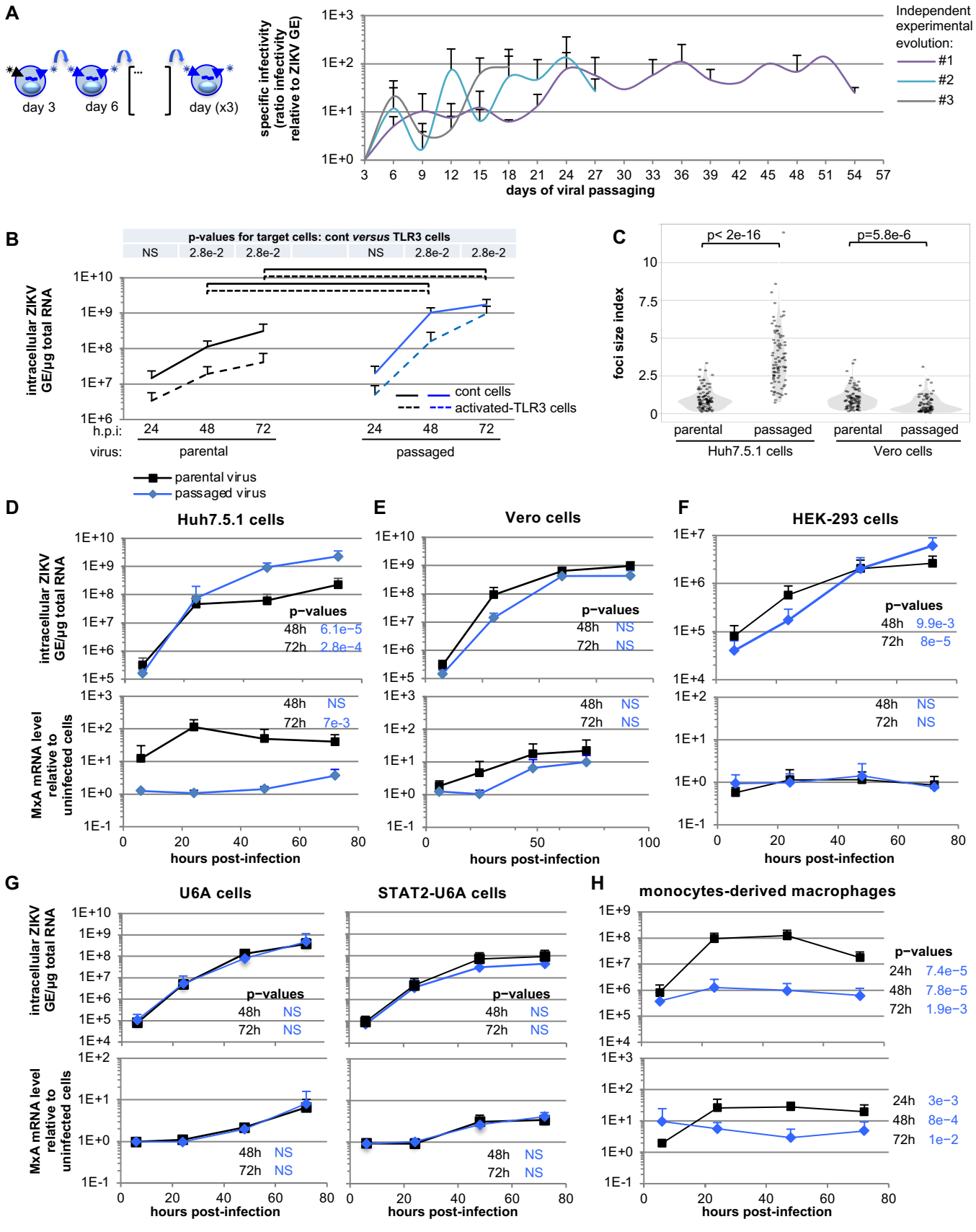
A
day 3
day 6
day (x3)
specific infectivity (ratio infectivity relative to ZIKV GE)
days of viral passaging
Independent experimental evolution:
#1
#2
#3
B
p-values for target cells: cont versus TLR3 cells
NS
2.8e-2
2.8e-2
NS
2.8e-2
2.8e-2
intracellular ZIKV GE/µg total RNA
h.p.i:
virus:
parental
passaged
cont cells
activated-TLR3 cells
parental virus
passaged virus
C
p< 2e-16
p=5.8e-6
foci size index
parental
passaged
Huh7.5.1 cells
Vero cells
D
Huh7.5.1 cells
E
Vero cells
F
HEK-293 cells
intracellular ZIKV GE/µg total RNA
MxA mRNA level relative to uninfected cells
p-values
48h 6.1e-5
72h 2.8e-4
48h NS
72h 7e-3
48h NS
72h NS
48h NS
72h NS
48h 9.9e-3
72h 8e-5
48h NS
72h NS
hours post-infection
G
U6A cells
STAT2-U6A cells
H
monocytes-derived macrophages
24h 7.4e-5
48h 7.8e-5
72h 1.9e-3
24h 3e-3
48h 8e-4
72h 1e-2

Figure 1

Figure 1. Increased specific infectivity and resistance to TLR3-mediated inhibition of serially passaged viral populations. A. As shown on the schematic representation of the experimental procedure for the serially passaging of ZIKV viral populations: every 3 days, viral supernatants were harvested, infectivity levels determined and, accordingly, used to infect naïve cells. Quantification of the specific infectivity (*i.e.*, defined as the probability for one physical virion to initiate infection) of the viral populations harvested over serially passaging in the course of 3 independent run of experimental evolution (referred to as #1, #2, #3 and stop at days 54, 21 and 18 respectively). Results are expressed as the ratio of the extracellular infectivity levels relative to extracellular ZIKV RNA levels and relative to day 3 for each independent passaging in control cells set to 1; 2-to-3 independent determination by RT-qPCR and infectious titrations for each evolution experiment; mean ± SD. **B.** Quantification of the intracellular ZIKV genome levels in kinetic analysis of serially passaged viral populations (*i.e.,* day 51 of the viral passaging) *versus* parental virus assessed in activated-TLR3 cells (dotted lines) as compared to control cells (solid lines) ; at the indicated times post-infection at MOI 0.05; 4 independent experiments; mean ± SD. The statistical comparison of intracellular ZIKV GE levels for the same viral population at the same time point post-infection between the target cells (*i.e.,* activated-TLR3 cells and control cells) is indicated in the table at the top of the graphs with indicated p-values and NS; $p>0.05$. The intracellular ZIKV GE levels at a same time post-infection between parental and passaged virus determined as significantly different ($p<0.05$) are indicated by brackets: dotted lines for the comparison of levels in activated-TLR3 cells and solid lines for the comparison of levels in control cells. **C.** Violin plot representation of the focus size at 48 hours post-infection by parental virus versus serially passaged virus (i.e., day 51 of the viral passaging) in Huh7.5.1 cells and Vero cells. The size index for each infectious focus is displayed by an individual dot; 5 independent measurements; statistical analysis as indicated by p-values. **D-H.** Kinetic quantification post-infection by parental versus serially passaged viral population (i.e., day 51 of the viral passaging) in Huh7.5.1 (**D**), Vero cells (**E**), HEK-293 cells (**F**), U6A cells and STAT2 expressing U6A cells (**G**) and macrophages derived from monocytes (**H**). Results present the levels of intracellular ZIKV GE (upper panels) and MxA (lower panels) mRNA levels relative to the levels in non-infected cells, at the indicated time post-infection at MOI 0.1; 3-to-7 independent experiments; mean ± SD. The p-values of the statistical analysis of the kinetics performed using mixed linear model are indicated on the right side of the graphs, p-value are for the comparison of passaged viral population versus parental virus, and NS; $p>0.05$.

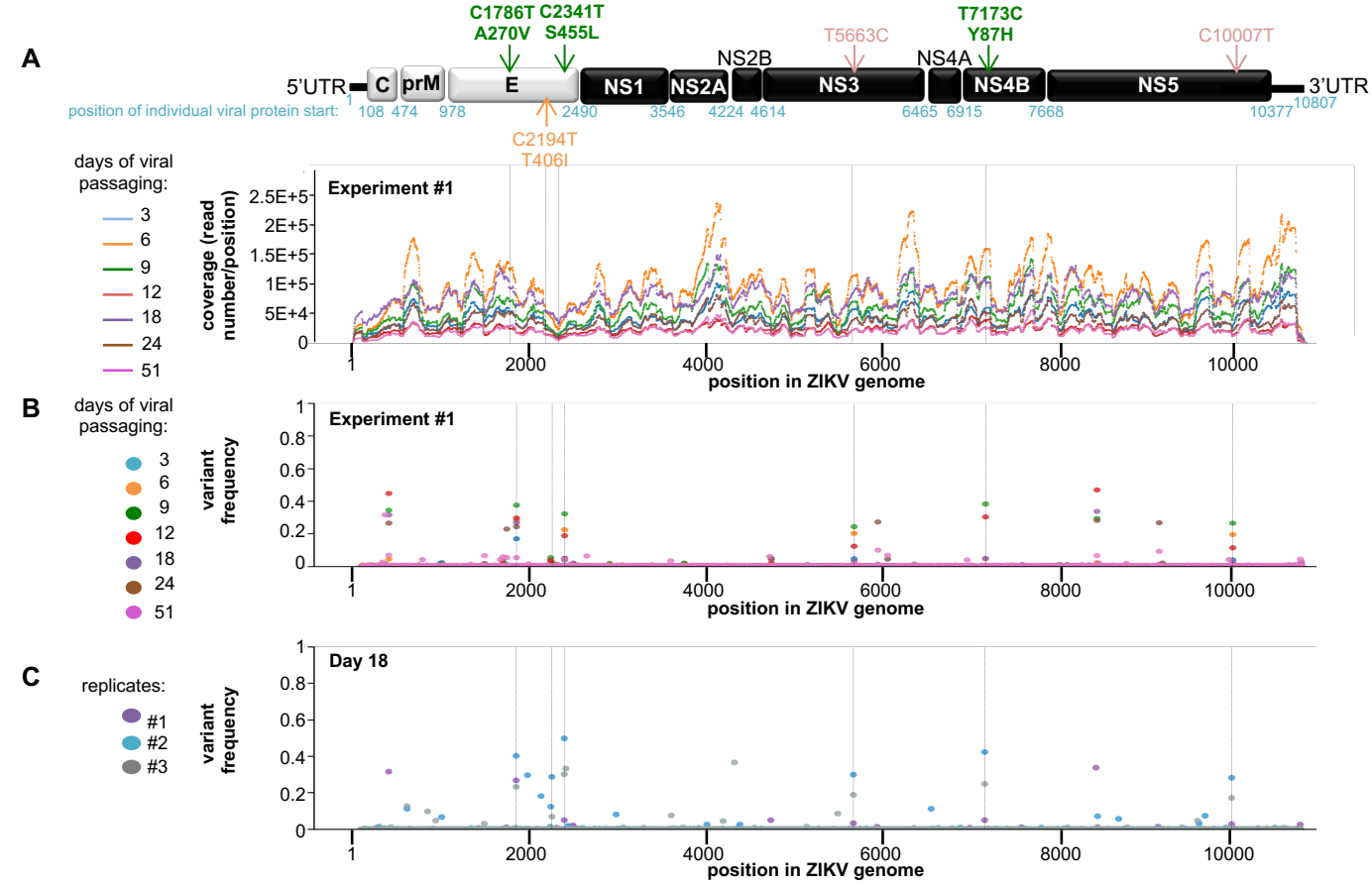
A
C1786T A270V
C2341T S455L
T5663C
T7173C Y87H
C10007T
5'UTR
C
prM
E
NS1
NS2A
NS2B
NS3
NS4A
NS4B
NS5
3'UTR
position of individual viral protein start:
1
108
474
978
2490
3546
4224
4614
6465
6915
7668
10377
10807
C2194T T406I
days of viral passaging:
3
6
9
12
18
24
51
coverage (read number/position)
Experiment #1
position in ZIKV genome
B
variant frequency
C
replicates:
#1
#2
#3
Day 18

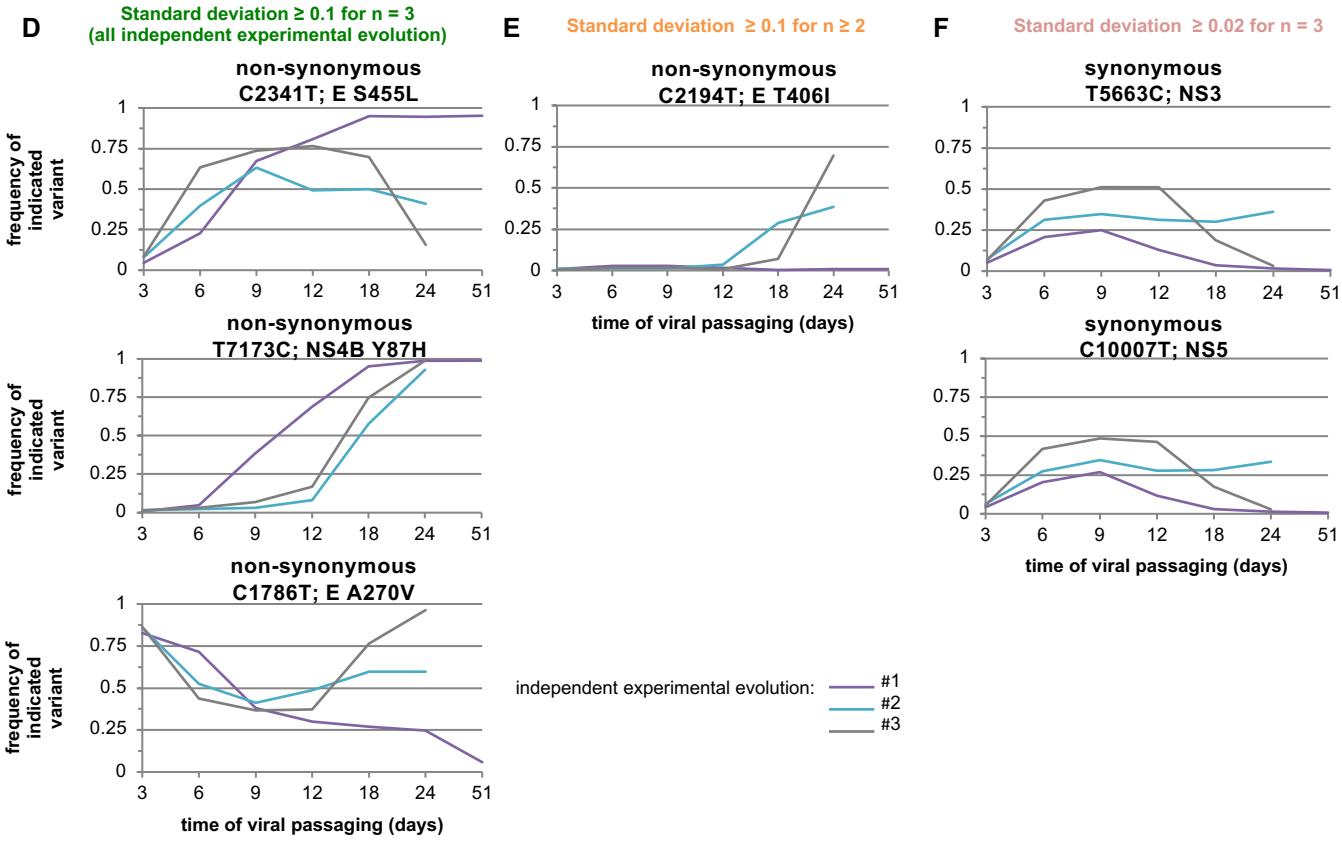
D
Standard deviation ≥ 0.1 for n = 3
(all independent experimental evolution)
E
Standard deviation ≥ 0.1 for n ≥ 2
F
Standard deviation ≥ 0.02 for n = 3
non-synonymous C2341T; E S455L
non-synonymous C2194T; E T406I
synonymous T5663C; NS3
non-synonymous T7173C; NS4B Y87H
synonymous C10007T; NS5
non-synonymous C1786T; E A270V
frequency of indicated variant
time of viral passaging (days)
independent experimental evolution:
#1
#2
#3

Figure 2

Figure 2. Bioinformatic analysis of the genetic evolution of viral populations obtained by next-generation sequencing. A. Coverage of the next-generation sequencing analysis along the ZIKV genome sequence of viral populations harvested at the indicated time points of the serial passaging of one representative independent run of evolution experiment. Results are expressed as number of reads per position; schematic representation of ZIKV genome at the top. **B-C.** Time-course quantification of the frequency of the second most frequent variants at each position along ZIKV genome in the viral populations harvested in one representative independent run of evolution experiment (**B**) and in the viral populations harvested at day 18 in 3 independent runs of evolution experiments (**C**). Dotted lines indicate the positions in the viral genome with high standard deviations in several runs of experimental evolution, as defined in **Fig S4. C. D-F.** Time-course quantification of the frequency of variants determined by next-generation sequencing. The variants were selected when the standard deviations of their frequencies were: ≥ 0.1 for all the 3 independent runs of experimental evolution (n =3; n referred to one replicate of one condition at given time of harvest) (**D**); ≥ 0.1 for a minimum of 2 samples (**E**), and ≥ 0.02 for a minimum of 3 samples (**F**), with thresholds defined according to the density of variants relative to their frequency for the pool of all analyzed samples, as presented in Fig S4. The variants are indicated as nucleotide position (*e.g.,* C2340T), the corresponding viral protein (*e.g*., E) and amino acid change for non-synonymous mutations (e.g., S455L); as also shown on the schematic representation of ZIKV genome organization (**A**).

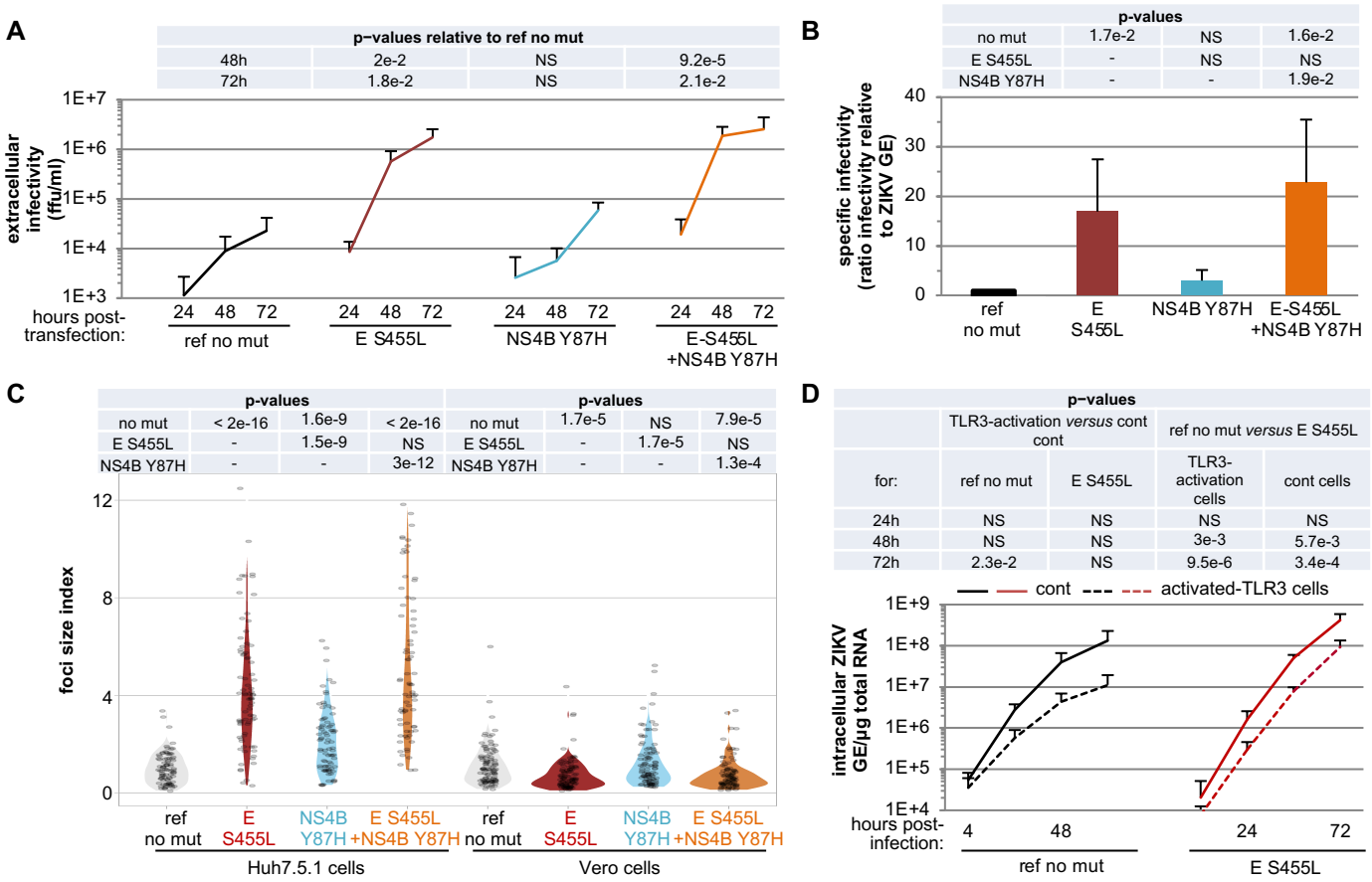

Figure 3. Introduction of the selected non-synonymous mutations in ZIKV molecular clone. ZIKV genome bearing the selected mutations (*i.e.,* single S455L mutation in E, Y87H in NS4B and combined E S455L and NS4B Y87H mutations), and as a reference ZIKV genome without the mutation (*i.e.,* ref no mut), were transfected in Huh7.5.1 cells. **A.** Time-course quantification of infectious viral production at the indicated times post-transfection. Results of 4-to-6 independent experiments; mean ± SD; p-values as indicated in the table above the graph and relative to the reference (ref no mut). **B.** Quantification of the specific infectivity (as in **Fig. 1A**) in the viral supernatants harvested at 72 hours for ZIKV genome mutants or not. Results are the mean ± SD relative to the reference virus set to 1 for each independent experiment; 4-to-6 independent experiments. The p-values indicated in the table correspond to one-by-one comparisons of the condition/mutant displayed below in the graph with conditions/mutants indicated on the left side of the table. **C.** Analysis of the focus size index of the indicated mutated or reference ZIKV determined in Huh7.5.1 and Vero cells, as indicated, for supernatants harvested at 72 hours post-transfection. The quantifications are displayed by violin plots, determined as in **Fig. 1C**. Results of 4 independent experiments; p-values as indicated in the table above the graph. **D.** Time-course analysis of the replication of the E S455L mutant versus reference virus (ref no mut) assessed in activated-TLR3 Huh7.5.1 cells (dotted lines) as compared to control cells (solid lines). Quantification of the intracellular ZIKV genome levels at the indicated times post-infection at MOI 0.005; 4 independent experiments; mean ± SD. The statistical comparison of intracellular ZIKV GE levels for the same target cells and between mutant and reference virus is indicated in the table at the top of the graphs with indicated p-values and NS; p>0.05.

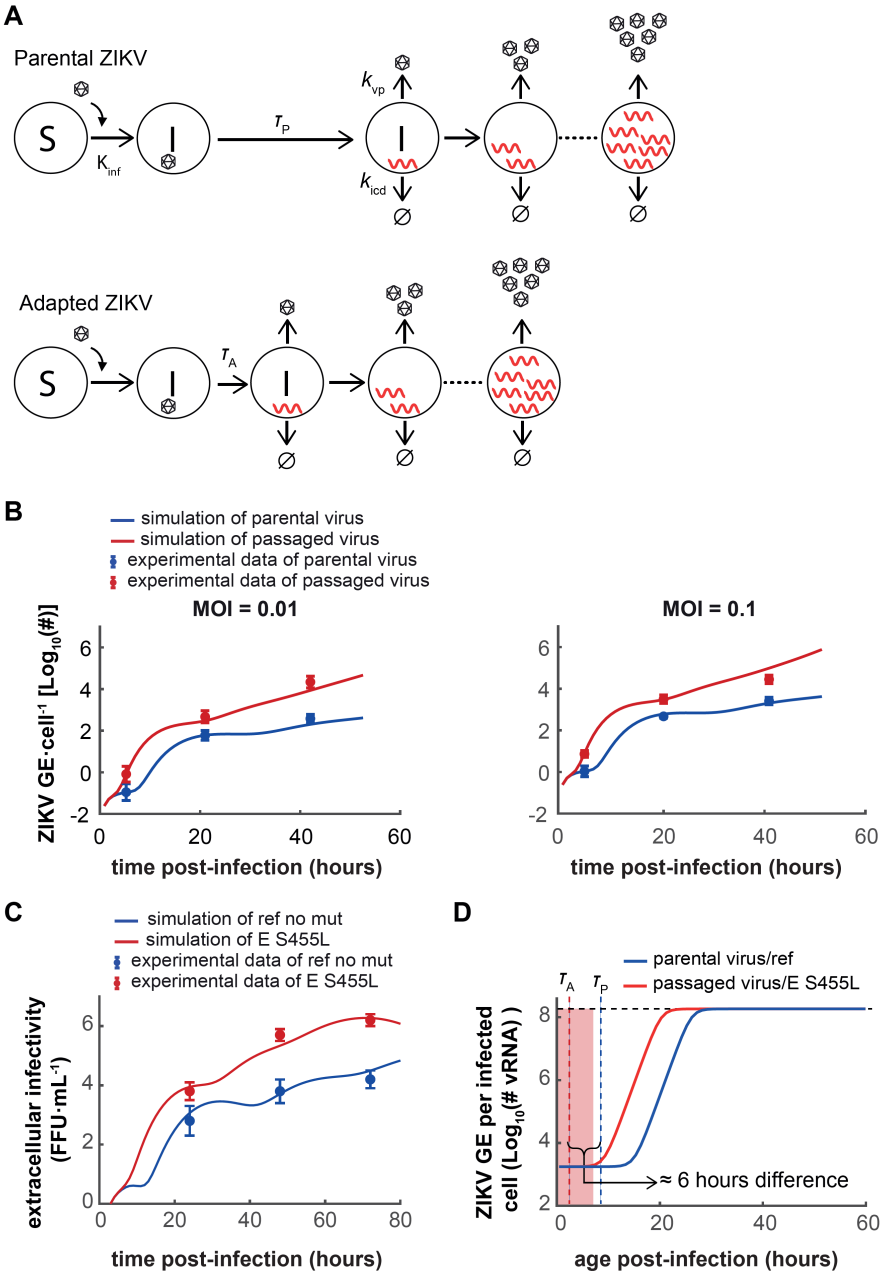

Figure 4. Multiscale model of ZIKV infection and replication. A. Schematic representation of the model. ZIKV infect susceptible cells with rate k_{inf}. Productive viral replication begins with a time delay τ_P for the parental virus and τ_A for the evolved or mutated viruses. Virus replication within infected cells is modeled as logistic growth (**Appendix 1,** mathematical model). Infected cells produce virions with rate k_{vp}, and die with rate k_{icd}. **B**. Model simulation with optimized parameters *versus* experimental measurements of the number of ZIKV genomes per cell upon infection with different doses of parental and adapted ZIKV. **C**. Model simulation *versus* experimental measurements of the number of foci-forming units (ffu) per ml of supernatant upon transfection with parental and the E S455L mutant ZIKV. **D**. Simulation of the ZIKV replication inside the infected cells for parental/ref and adapted/E S455L mutant. The shaded region is the 95% CI for the estimated τ_A value.